ICES Journal of Marine Science

ICES Journal of Marine Science (2015), 72(2), 388–402. doi:10.1093/icesjms/fsu090

Original Article

Model study of nutrient and phytoplankton dynamics in the Gulf of Maine: patterns and drivers for seasonal and interannual variability

Rucheng Tian[1*‡], Changsheng Chen[1], Jianhua Qi[1], Rubao Ji[2], Robert C. Beardsley[3], and Cabell Davis[2]

[1]*School for Marine Science and Technology, University of Massachusetts-Dartmouth, 706 South Rodney French Blvd, New Bedford, MA 02744, USA*
[2]*Department of Biology, Woods Hole Oceanographic Institution, Woods Hole, MA 02543, USA*
[3]*Department of Physical Oceanography, Woods Hole Oceanographic Institution, Woods Hole, MA 02543, USA*

**Corresponding author: tel: +1 410 295 1328; fax: +1 410 267 5777; e-mail: rtian@chesapeakebay.net.*
‡*Present address: UMCES/CBPO, 410 Severn Avenue, Annapolis, MD 21403, USA.*

Tian, R., Chen, C., Qi, J., Ji, R., Beardsley, R. C., and Davis, C. Model study of nutrient and phytoplankton dynamics in the Gulf of Maine: patterns and drivers for seasonal and interannual variability. – ICES Journal of Marine Science, 72: 388–402.

Received 25 September 2013; revised 23 April 2014; accepted 24 April 2014; advance access publication 10 June 2014.

Coupled physical–biological modelling experiments were made for the period of 1995–2009 to analyse the spatial and interannual variability of nutrients and phytoplankton production in the Gulf of Maine (GOM). The physical model was the Finite-Volume Community Ocean Model (FVCOM) and the biological model was a Nitrogen, Phytoplankton, Zooplankton, and Detritus (NPZD) model. The simulation was carried out with realistic meteorological surface forcing, five major tidal constituents, river discharge, and observation-based open boundary conditions. The results were robust with comparison to SeaWiFS chlorophyll data and historical data of nitrogen. An Empirical Orthogonal Function analysis clearly identified two dominant modes in nutrient and phytoplankton dynamics: (1) sustained nutrient supply and phytoplankton production from spring through autumn, and (2) a dominating phytoplankton bloom in spring, relatively low production in summer, and a noticeable bloom in autumn. Mode 1 was a dominant feature in strong tidal energy dissipation regions such as the southwestern shelf of Nova Scotia, Georges Bank, Nantucket Shoals, the Bay of Fundy, and the coastal regions of GOM, where tidal pumping and mixing were the major drivers for the sustained nutrient supply, and primary production showed certain resilience with less interannual variability. Mode 2 was a characteristic in the deep Gulf, the offshore region of the Scotian Shelf, and in the open sea area, where the timing and amplitude of the spring phytoplankton bloom is essentially controlled by the salinity regime, and its interannual variability was significantly influenced by freshening events controlled by local and remote forcing.

Keywords: Gulf of Maine, interannual variability, modelling, nutrient, phytoplankton.

Introduction

The Gulf of Maine (GOM) is a semi-enclosed continental shelf sea in the northeastern coastal region of North America, with a connection to the Northwest Atlantic Basin through the Northeast Channel (NEC) between Georges Bank (GB) and Nova Scotia (Figure 1). In the shallow coastal region, the subtidal circulation is dominated by a general anticlockwise circulation with waters entering from the Scotian Shelf, flowing from the eastern GOM coast (defined as the Eastern Maine Coastal Current, EMCC) to the western GOM coast (defined as the Western Maine Coastal Current, WMCC) and exiting onto the southern New England Shelf (NES) through the Great South Channel (Figure 2; Beardsley *et al.*, 1997). GB is a shallow submarine bank dominated by a permanent clockwise residual circulation (Butman *et al.*, 1982), and the intensity of this circulation varies significantly with season due to seasonal variability of the tidal mixing front and water transport across the NEC (Chen *et al.*, 1995; Smith *et al.*, 2003).

The interannual variability of the GOM circulation is controlled by both local and remote forcing, the former comprising air–sea interaction and river discharges (Geyer *et al.*, 2004) and the latter due to slope transport connected to the Labrador Current (Chapman and Beardsley, 1998) and onshore meandering of the

Gulf Stream (Garfield and Evans, 1987; Ryan *et al.*, 2001). Due to the resonant nature of the M_2 tide in the GOM system (Garrett, 1972), the changes of local and remote forcing plus strong tidal mixing characterize the physical environment that drives the spatial and temporal variations of this coastal system.

The GOM/GB is known as a productive ecosystem, with primary production ranging from 180 to 400 g C m^{-2} $year^{-1}$ (O'Reilly *et al.*, 1987). GB is characterized by an around-bank recirculation and the tidal mixing front which separates the central vertically mixed region from the peripheral stratified region. Nutrient cross-frontal transport (also known as "tidal pumping") is the key mechanism to sustain high primary production (Franks and Chen, 1996; Hu *et al.*, 2008). Garrett and Loder (1981) listed five mechanisms responsible for cross-frontal transport: mean flow flux, shear dispersion, barotropic eddies, baroclinic eddies, and wind-driven transport. Marsden (1986) reported that internal tide instability and breaking played a large role in determining cross-isobath scalar transports. Horne *et al.* (1989) found that the cross-frontal transport of nitrogen was well in excess for biological demand on GB owing to non-linear interactions and nutrient gradient and mixing. Loder and Horne (1991) did an analytical study on the mechanisms controlling cross-isobath transport. They defined the eddy flux of a scalar in a time-dependent rotary velocity field as the "skew flux", which essentially consists of the transport by the Stokes velocity and contributes to the cross-isobath transport of nutrients on GB. Topographic rectification of barotropic tidal current and baroclinic–barotropic tidal current interaction also can drive cross-isobath transport. In addition to strong non-linear interactions, Chen and Beardsley (2002) combined this asymmetric tidal mixing with varying windforcing and chaotic mixing associated with cross-frontal water exchange to explain cross-isobath transport on GB. Ji *et al.* (2008) found using a coupled biophysical model that cross-frontal fluxes were modulated by stratification, surface windstress, and the initial nutrient concentration in the GOM source waters (Figure 1, SR6–SR9).

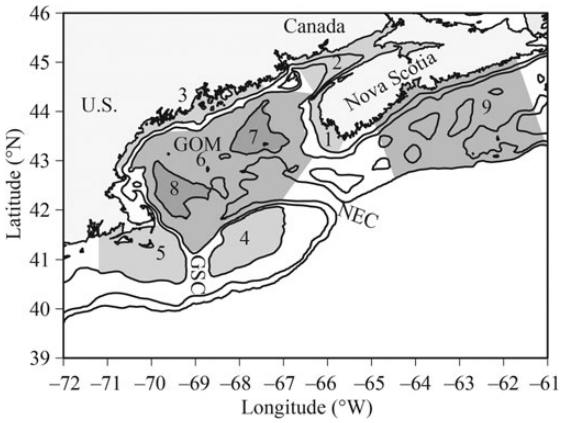

Figure 1. The GOM study area with the Scotian Shelf to the northeast and the eastern NES to the southwest. Subregions are defined here based on tidal energy analysis (Chen *et al.*, 2011): SR1, southwestern Scotian Shelf; RS2, Bay of Fundy; SR3, GOM coast; SR4, GB; SR5, NS; SR6, GOM (>100 m); SR7, Jordan Basin; SR8, Wilkinson Basin; and SR9, Scotian Shelf. Subregions SR1–SR5 are tidal mixed regions, whereas tidal mixing is relatively weak in the GOM (SR6) and its two deep basins (SR7 and SR8) and the Scotian Shelf (SR9). Continuous lines are the 60, 100, and 200 m isobaths. The deep channel on the northeastern side of GB (SR4) is the NEC and the channel between GB (SR4) and NS (SR5) is the Great Southern Channel (GSC).

This region constitutes important fishing grounds, including multiple groundfish species, sea scallops, and shrimps. Intense attention has been paid to phytoplankton blooms, not only for understanding the impact of physical variability on lower trophic level dynamics (Franks and Chen, 1996, 2001; Ji *et al.*, 2006, 2008) but also their direct effects on fishery recruitment in the region (Platt *et al.*, 2003; Header *et al.*, 2005; Friedland *et al.*, 2008). Franks and Chen (1996) pioneered a coupled physical–biological primitive equation model to demonstrate how tidal-induced advection and mixing pump nutrients up towards the tidal mixing front and fuel phytoplankton production on GB. Ji *et al.* (2008) conducted a process-oriented modelling experiment to examine the impact of freshwater inflow through the Scotian Shelf on the timing and productivity on the spring phytoplankton bloom in GOM. They found that freshening could lead to an earlier but small bloom as a result

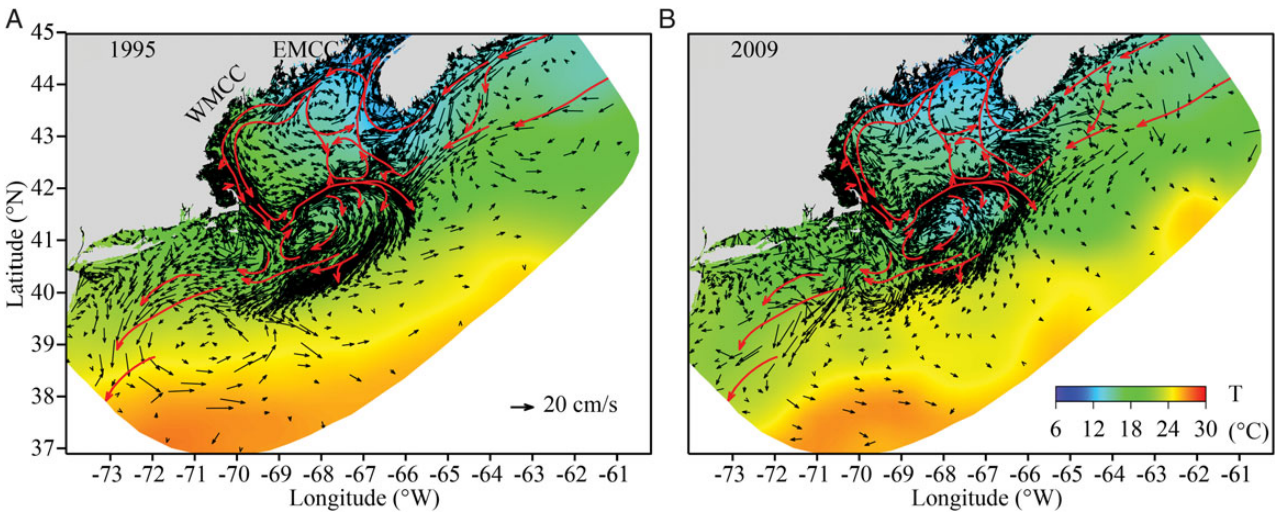

Figure 2. Simulation domain, long-term subtidal surface current in summer (red lines; Beardsley *et al.*, 1997) and monthly averaged surface current in July 1995 (starting year) and 2009 (ending year) of our simulation. EMCC, Eastern Maine Coastal Current; WMCC, Western Maine Coastal Current.

of enhanced stratification and reduced nutrient flux from the deeper region to the euphotic zone.

The previous studies have provided conceptual insights into the response of the phytoplankton dynamics to local and remote variability of physical conditions in the GOM/GB region. Due to unavailability of long-term simulations of the physical field, however, no modelling studies were carried out to simulate nutrients and phytoplankton and their variability over seasonal and interannual time-scales. Our understanding of interannual variability of phytoplankton in this region is mainly based on time-series of satellite-derived remote sensing images and field measurement data. Since field measurements were sparse, and the region is often very cloudy, a multiyear model validated with available observational data is needed for a better understanding of the dynamics controlling the spatial and temporal variability of phytoplankton in the GOM/GB region.

The University of Massachusetts-Dartmouth (UMASSD) and Woods Hole Oceanographic Institution (WHOI) joint research team has developed a high-resolution model for the GOM/GB region (Chen *et al.*, 2006, 2011; Cowles *et al.*, 2008) and used it to simulate the physical field over the period of 1995–2009. Driven by the assimilated physical fields, we have run a lower trophic foodweb model for the same period. The goals of our simulation are aimed at (i) studying the response of nutrient-plankton dynamics to different physical forcing conditions and (ii) discerning the major physical and biological factors responsible for the seasonal and interannual variability in biological productivity in the region. Built on a reasonable agreement between modelled and observed nutrient and chlorophyll concentrations, we have conducted Empirical Orthogonal Function (EOF) and correspondence analyses (CA) to examine the dynamical characteristics of the lower trophic foodweb system in space and time over the past decade and distinguish the biological regimes that are influenced predominantly by local and remote forcing.

The model and design of numerical experiments

Physical model

The physical model used to drive the biological model is the three-dimensional primitive equation unstructured-grid, general terrain-following coordinate, Finite-Volume Community Ocean Model (FVCOM) developed originally by Chen *et al.* (2003) and upgraded by the team effort (Chen *et al.*, 2006, 2007, 2008, 2011; Lai *et al.*, 2010; Gao *et al.*, 2011). FVCOM is discretized with an integral form of governing equations over momentum and tracer control volumes and is integrated with time by a mode-split solver in which external and internal modes are advanced in tandem at different time-steps (Chen *et al.*, 2003). In the horizontal, FVCOM uses a non-overlapping unstructured triangular grid with an advantage of resolving the complex coastal geometry in the GOM. In the vertical, FVCOM uses a terrain-following hybrid coordinate, in which the water column is divided into 30 layers and the resolution is 1.0 m or less in the shallow regions. Vertical turbulent mixing is calculated using the General Ocean Turbulence Model (GOTM) libraries (Burchard and Bolding, 2001; Tian and Chen, 2006), with the 2.5 level Mellor-Yamada turbulence model set as the default (Mellor and Yamada, 1982).

The numerical domain of FVCOM covers the GOM/GB/NES region and is enclosed by an open boundary running from the New Jersey shelf to the Nova Scotia shelf (Figure 2). The horizontal resolution is ∼1.0–2.0 km around the shelf break of GB and near the coastal region, 2–3 km over the top of GB, and ∼10–15 km in the interior of the GOM and near the open boundary. A hindcast experiment was conducted from 1995 to 2009, in which the model was driven by winds, net heat flux plus vertical penetration of shortwave irradiance computed by the mesoscale meteorological models (MM5 for the period of 1995–2006 and WRF for the period of 2007–2009) at the surface, tidal forcing (constructed using five tidal constituents: M2, S2, N2, O1, and K1) at the open boundary, and freshwater discharge from the primary rivers. The inflow from the Nova Scotia shelf was computed using a sea surface slope determined from observed density distribution and Ekman transport from local windforcing. Data assimilation of SST and available hydrographic profiles was conducted daily (Chen *et al.*, 2009). A series of data-model comparison were made to validate this model (e.g. Cowles *et al.*, 2008; Lai *et al.*, 2010; Chen *et al.*, 2011; Xue *et al.*, 2012).

To illustrate the robustness of the physical simulation, simulated currents averaged over July are plotted together with the synthesized summer residual current by Beardsley *et al.* (1997). Examples of 1995 (starting year) and 2009 (ending years) are included (Figure 2). All the major currents and circulation systems are resolved, including the Scotian Shelf inflow, the anticlockwise coastal circulation around the coast of the GOM, the clockwise recirculation gyre around GB, and the outflow through the Great South Channel to the Mid-Atlantic Bight. For detailed interpretation of the simulated physical fields, readers are referred to Cowles *et al.* (2008), Lai *et al.* (2010), Chen *et al.* (2011), and Xue *et al.* (2012).

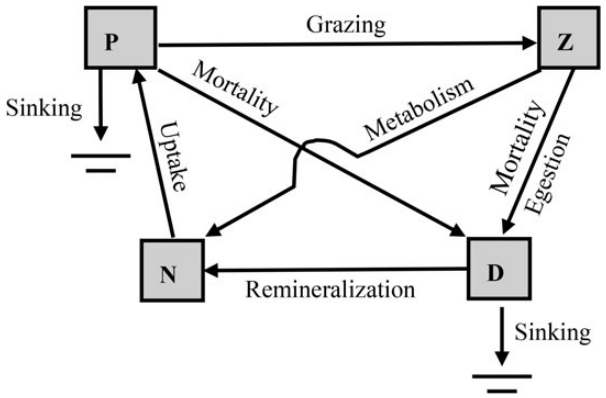

Figure 3. NPZD model structure and energy flow.

Biological model

The NPZD model consists of four state variables: Nitrogen (N; dissolved inorganic nitrogen), Phytoplankton (P), Zooplankton (Z), and Detritus (D) and six processes controlling trophic links and remineralization (Figure 3). The model unit is mmol N m^{-3} for all the state variables. Phytoplankton biomass (P) is controlled by growth (U_P), grazing (G_Z), mortality (m_p), and sinking (s_p):

$$\frac{dP}{dt} = U_P - G_Z - m_p f(T)P^2 + s_P \frac{\partial P}{\partial z}. \quad (1)$$

Phytoplankton growth is regulated by nitrogen limitation [$f(N)$], photosynthetically active radiation [$f(I)$], and temperature

$[f(T)]$ expressed mathematically as:

$$U_P = \mu_{\max} f(N) f(I) f(T) P, \tag{2}$$

where $\mu_{\max}$ is the maximum growth rate of phytoplankton. Limitation of phytoplankton growth by nitrogen is formulated using the Michaelis–Menten kinetics:

$$f(N) = \frac{N}{N + K_N}, \tag{3}$$

where K_N is the half-saturation constant. Light forcing on phytoplankton growth is parameterized using the Platt *et al.* (1980) formulations:

$$f(I) = (1 - e^{-\alpha I/\mu_{\max}}) e^{-\beta I/\mu_{\max}}, \tag{4}$$

where α and β are the light-growth slope and inhibition coefficient and I represents the photosynthetically active radiation (PAR) and its attenuation in the water column is calculated as a function of water depth (z), phytoplankton (P), and detritus (D) concentration given as:

$$I(z) = I_0 \exp\left(-k_W z - k_P \int_{-z}^{0} P\,dz - k_D \int_{-z}^{0} D\,dz\right), \tag{5}$$

where I_0 is PAR at the sea surface and k_W, k_P, and k_D are the attenuation coefficients of water, phytoplankton, and detritus, respectively. Temperature effect on phytoplankton growth and other biological rates is parameterized as an exponential function:

$$f(T) = e^{-a|T - T_{\text{opt}}|}, \tag{6}$$

where a and T_{opt} are the coefficient and optimal temperature. Zooplankton grazing is formulated as:

$$G_Z = \frac{g_{\max} f(T) Z P^2}{P^2 + K_P^2}, \tag{7}$$

where $g_{\max}$ is the zooplankton maximum grazing rate and K_P the half-saturation constant for zooplankton grazing.

The zooplankton biomass is then determined by growth efficiency (γ) and mortality (m_z):

$$\frac{dZ}{dt} = \gamma G_Z - m_z f(T) Z^2, \tag{8}$$

where γ is the assimilation coefficient and m_z the mortality coefficient.

Nitrogen is taken up by phytoplankton and produced through remineralization of biogenic detritus and zooplankton metabolism:

$$\frac{dN}{dt} = -U_P + \lambda G_Z + \varepsilon f(T) D, \tag{9}$$

where λ is the active respiration zooplankton expressed as a fraction of grazing and ε the remineralization rate of detritus.

Detritus is formed through phytoplankton and zooplankton mortality and egestion and remineralized into nitrogen:

$$\frac{dD}{dt} = (1 - \gamma - \lambda) G_Z + m_p P^2 + m_z Z^2 - \varepsilon f(T) D + s_D \frac{\partial D}{\partial z}. \tag{10}$$

The NPZD model represents an aggregated compartment model with simplified biological processes. At the phytoplankton level, the model is not species-specifics such as differences in growth rate and nutrient demand. Phytoplankton respiration is not explicitly simulated, but integrated into the grazing and mortality terms. As presented later, 30% of the grazing amount is directly converted into inorganic nitrogen and biogenic detritus from phytoplankton mortality is constantly mineralized into inorganic nitrogen. Both the grazing and the mineralization rate depend on temperature forcing. Only nitrogen is considered in the model and nutrient limitation by silicate and phosphorus is not included. The zooplankton compartment serves as a closure term that mimics the grazing pressure on phytoplankton. Differences in zooplankton species are not taken into account, and predation from higher trophic level is combined in the mortality terms. Despite these simplifications and aggregations, the NPZD model has demonstrated its capability of simulating the basic ecosystem process at the low trophic level (Ji *et al.*, 2008). We chose this model with an aim at identifying physical drivers for interannual variability of nutrients and phytoplankton. For this purpose, species-specific properties are beyond the scope of our consideration.

Parameter definition, units, and values were described in detail in Ji *et al.* (2008) and Tian *et al.* (2001) (Table 1). The phytoplankton maximum growth rate ($\mu_{\max}$), light photosynthesis slope (α), and light inhibition coefficient (β) are assigned together to fit the photosynthesis–irradiance curve observed in the region (Ji *et al.*, 2006).

Table 1. Parameter definition, values, and units of the NPZD model (Ji *et al.*, 2008).

Symbol	Definition	Value	Unit
N	Nitrogen	Variable	mmol N m^{-3}
P	Phytoplankton	Variable	mmol N m^{-3}
Z	Zooplankton	Variable	mmol N m^{-3}
D	Detritus	Variable	mmol N m^{-3}
a	Temperature coefficient	0.07	$^{\circ}C^{-1}$
$g_{\max}$	Maximum grazing	$0.81e^{-5}$	s^{-1}
k_C	Light attenuation by phytoplankton	0.06	m^2 (mmol N)$^{-1}$
k_D	Light attenuation by detritus	0.01	m^2 (mmol N)$^{-1}$
k_W	Light attenuation by pure water	0.08	m^{-1}
K_N	Half-saturation constant for nitrogen uptake	0.5	mmol N m^{-3}
K_P	Half-saturation constant for grazing	0.25	mmol N m^{-3}
m_p	Phytoplankton mortality	$9.26e^{-7}$	s^{-1} (mmol N m^{-3})$^{-1}$
m_z	Zooplankton mortality	$6.94e^{-7}$	s^{-1} (mmol N m^{-3})$^{-1}$
s_P	Phytoplankton sinking speed	$1.157e^{-5}$	m s^{-1}
s_D	Detritus sinking speed	$1.157e^{-4}$	m s^{-1}
T_{opt}	Optimal temperature	$^{\circ}C$	20
$\mu_{\max}$	Phytoplankton maximum growth rate	$3.25e^{-5}$	s^{-1}
α	Light-photosynthesis slope	$1.62e^{-6}$	m^2 s^{-1} w^{-1}
β	Light inhibition coefficient	$3.24e^{-8}$	m^2 s^{-1} w^{-1}
ϵ	Remineralization rate at 0°C	$1.736e^{-7}$	s^{-1}
λ	Active respiration	0.3	Dimensionless
γ	Zooplankton growth efficiency	0.4	Dimensionless

The phytoplankton mortality (m_p) is set as 9.26×10^{-7} s^{-1}, which is equivalent to 8% d^{-1}. Note that this value includes the loss of the total phytoplankton biomass other than zooplankton grazing, such as respiration and DOM exudation. The half-saturation constant for nitrogen uptake is assigned to 0.5 mmol m^{-3} for the bulk phytoplankton compartment. Zooplankton maximum grazing rate (g_{max}) is set to 0.81×10^{-5} s^{-1} (0.7 d^{-1}). The active respiration of zooplankton intake (λ) is set to 0.3, whereas the growth efficiency (γ) is 0.4. This means that 30% of the grazing is converted to inorganic nitrogen through metabolism, 40% is used to grow, and the remained 30% is channelled to detritus through sloppy feeding and egestion. The mortality of zooplankton (m_z) is assigned to 6% d^{-1}, including the predation loss by higher trophic predators. All the biological processes are subject to temperature with an exponential coefficient (a) of 0.07, so that the biological response is doubled over each 10°C increase in temperature. As the same temperature parameter values were used due to the lack of information specific to each process in the region, different responses to temperature forcing from zooplankton and phytoplankton were not resolved in this application. Although, light attenuation is linked to phytoplankton and detritus shading, the detritus D in Equation (5) represents only dead biological materials. Any sediment resuspension and mineralization linked to tidal energy dissipation were not modelled. On the other hand, the attenuation coefficient by water (k_w) is assigned to 0.08 m^{-1}, which is significantly higher than that of pure water and was thus designed to capture attenuation by suspended sediment and dissolved materials. Using this parameter set, the model is able to reproduce the observed nitrogen and chlorophyll fields described later in the paper. While the model structure, biological processes, and parameterizations are highly simplified, the results compare well with the field data. Future studies are needed to examine more complex model structure and evaluate the full parameter space.

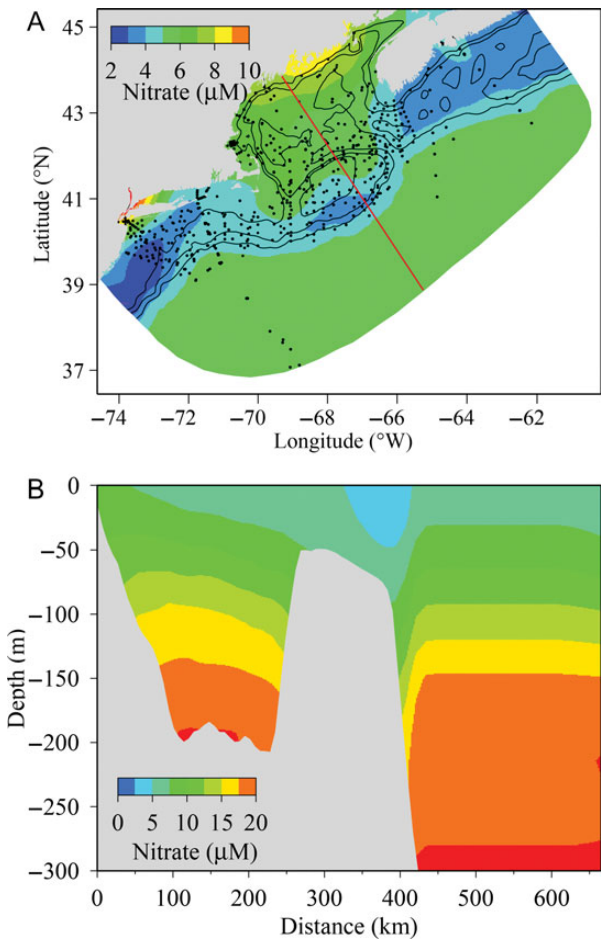

Figure 4. Nitrogen initial condition based on historical data and OA.

Initial and boundary conditions for the NPZD model

The initial condition of nitrogen was specified using the December climatological data obtained through an objective analysis (OA; Figure 4). Data sources include the National Oceanographic Data Center (www.nodc.noaa.gov), the Canadian Marine Environmental Data Service (MESD, provided by Dr Pierre Clement) and the University of Maine Database (provided by Dr Dave Townsend). In total, 1398 data profiles were gathered for December. The OA was done using the software developed by Bedford Institute of Oceanography (Hendry and He, 1996). In this software, the covariance function (R) between data and estimation sites is calculated with a function of the pseudo-distance (r) given as

$$R(r) = \left(1 + r + \frac{r^3}{3}\right)e^{-r}, \tag{11}$$

$$r = \sqrt{\left(\frac{x_d - x_m}{a}\right)^2 + \left(\frac{y_d - y_m}{b}\right)^2 + \left(\frac{z_d - z_m}{c}\right)^2 + \left(\frac{t_d - t_m}{T}\right)^2}, \tag{12}$$

where x, y and z are the eastward, northward, and upward axes of the Cartesian coordinate system; t denotes the time; the subscripts d and m indicate data and model positions, respectively; and parameters a, b, c, and T are the de-correlation scales for their corresponding coordinate. Given the sparse data, particularly in the open sea regions, the relatively large de-correlation scale of 100 km was

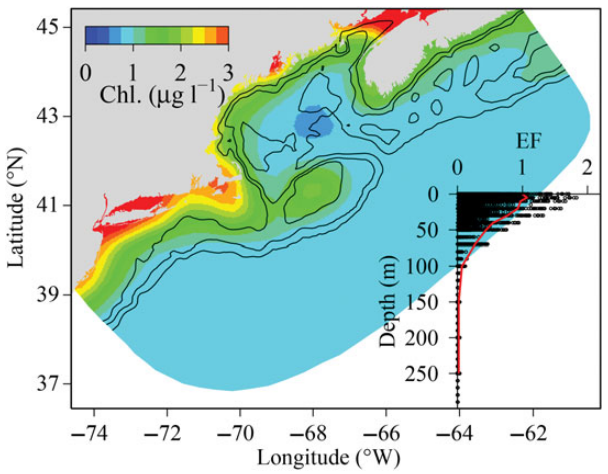

Figure 5. Phytoplankton initial condition based on SeaWiFS data and vertical extrapolation profile shown in lower right. The extrapolation factor (EF) profile (red line) was determined as the ratio of the average chlorophyll concentration of a specific layer over the average of the surface layers calculated from all the historical data in December (black dots).

used for a and b. In the vertical, the data were first interpolated onto standard levels, so that the depth de-correlation scale c was assigned to 1 m. The de-correlation time-scale term in Equation (6) was not taken into account, so that all the data in the month were equally weighted.

The resulting initial field of nitrogen was relatively homogenous in the horizontal (Figure 4 upper panel), with slightly higher values near the eastern Maine coastal area and slightly lower values along the shelf break region and over the Scotian Shelf. In the vertical, the nitrogen concentration increased with depth: 2–8 μM near the surface in the interior and ∼10 μM in the coastal region and >18 μM below 150 m (Figure 4 lower panel). Over the southern flank of GB, low concentration <5 μM appeared in the region between the shelf break and 40-m isobath.

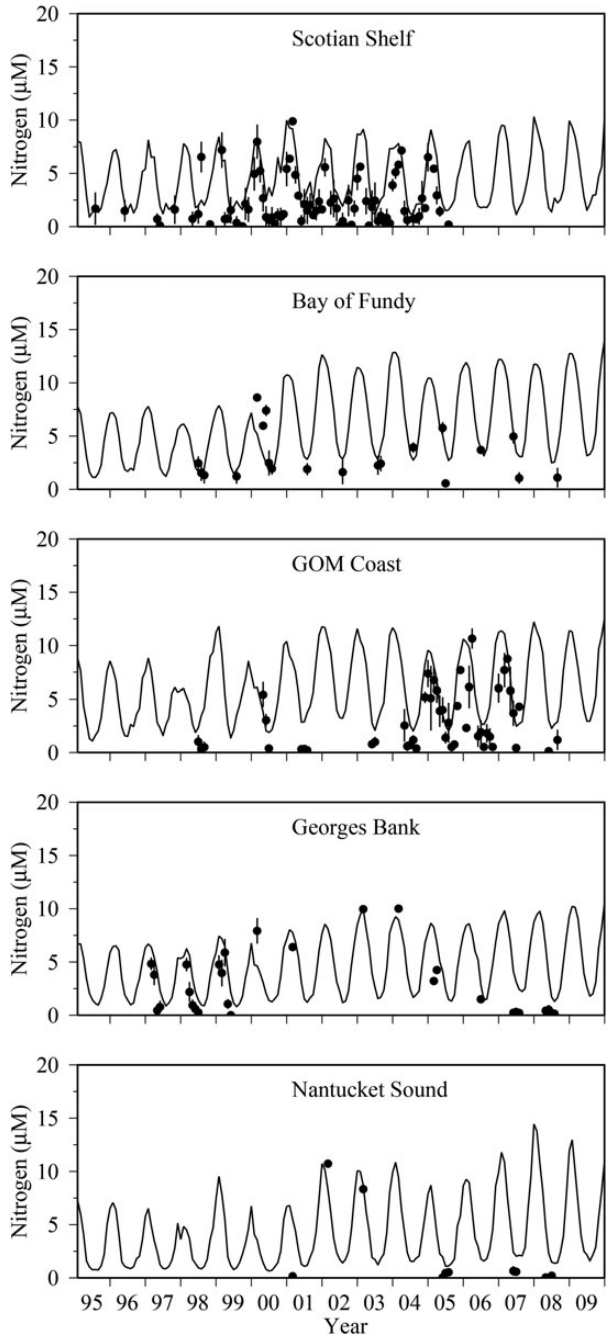

Figure 6. Model-predicted nitrogen (lines) vs. historical data (dots) in the surface layer in the five subregions SR9 and SB2 – SR5. Vertical bars indicate the standard deviation.

The initial condition of phytoplankton was determined based on historical and SeaWiFS-derived chlorophyll concentrations with an assumption of a carbon to chlorophyll ratio of 50 and the Redfield C:N ratio of 6.625 (Anderson, 2009). First, an average profile of the chlorophyll concentration in the computational domain was constructed from the available December climatological data (Figure 5). Then, the 9-km resolution SeaWiFS-derived chlorophyll concentration data were extrapolated into the water column according to the averaged profile of historical data. The extrapolated dataset was finally interpolated on the simulation grid using the OA mapping. The chlorophyll concentration in December was at a relatively low level: $<1\ \mu g\ l^{-1}$ in most of the computational domain and in a range of $1-3\ \mu g\ l^{-1}$ in the coastal regions and embayments. Slightly higher chlorophyll concentration was observed over GB. Few data were available for zooplankton biomass and biogenic detritus, so that the constant values of 0.4 and 0.2 mmol N m^{-3} were specified, respectively. These values were spatially modified in the equilibrium run after 5-year spinning-up simulation. The simulated zooplankton biomass ranges from 0.2 to 0.8 mmol N m^{-3} and that of detritus were not well recorded due to sinking in the water column. As mentioned in the previous section, these two terms represent model closures, so that detailed results are not presented in this paper. As these values are relatively small compared with nitrogen concentration, it is unlikely that the initial values of zooplankton and detritus can significantly alter the nitrogen mass balance in the whole system.

The open boundary condition of nitrogen was constructed for each month using the historical data through the OA mapping. Since data were too sparse for phytoplankton, zooplankton, and detritus, a data-based open boundary condition cannot be established. In the case when the current flows from inside to outside of the domain, concentrations at the boundary nodes are determined by the mass balance among all the biological and physical terms, the same way as a regular node inside the domain. When the current flows towards the inside of the domain, the concentration at the previous time-step was used at the open boundary node. Nutrient inputs from the rivers were determined by historical data.

Numerical experiment and data analysis

The biological model was driven by the FVCOM hourly output fields, with an integration time-step of 120 s. The two successive hourly physical fields were linearly interpolated to the biological time-step, with a recalculation of continuity equation to ensure the volume conservation. Using the aforementioned initial and boundary conditions, the model was first spun up 5 years using the 1995 physical forcing to reach an annual equilibrium state and then run continuously from 1995 to 2009.

Model output was validated with SeaWiFS and historical chlorophyll data. A Taylor diagram was constructed based on observed nitrogen and monthly SeaWiFS chlorophyll data. Basically, a Taylor diagram displays the correlation coefficient, standard deviation, and centred root-mean-square error (RMSE) between observations and model results on the same arc diagram (Taylor, 2001). The correlation coefficient (R) between modelled and observed values is given by the azimuthal position (A):

$$A = \cos^{-1}(R). \tag{13}$$

The standard deviation is proportional to the radial distance from the origin and the RMSE the distance between the modelled and observed values in the diagram with the same unit of standard deviation (Taylor, 2001). Given that the standard deviation of observed data varied from year to year, normalization was performed using the standard deviation of the observation (Fennel *et al.*, 2006).

EOF analysis was performed on monthly averaged primary production results. Given the heterogeneity of biological fields, normalization on the raw data were first performed on each node by subtracting the temporal mean, and then, dividing the data by the standard deviation obtained from the same node over the full dataset (Yoder *et al.*, 2002). Singular value decomposition was used to obtain the dominant EOF modes and principal components. Further, CA were conducted to link the timing and amplitude of the spring phytoplankton bloom with environmental factors such as the surface mixed layer depth, temperature, salinity, nitrogen concentration, and zooplankton biomass. CA can reveal not only the dependence between variables, but also their temporal evolution over the years analysed in the model (Gottelli and Ellison, 2004). The amplitude of the bloom was defined as the maximum chlorophyll concentration and the timing was defined as the day of the year when the maximum chlorophyll concentration occurred. While the timing of the bloom varied each year, the environmental condition averaged in February was used as a pre-bloom condition. CA was performed on the normalized dataset to avoid bias caused by variable units.

Results

Nitrogen

Nitrogen simulation was first compared with data in terms of regional monthly average in the surface layer (<10 m) in the shallow regions (SR2–SR5; Figures 1 and 6) and the surface layer and deep layer (>100 m) in the Gulf (SR6; Figure 7). The simulation is broadly comparable with the data in terms of magnitude and seasonal variations. The model reproduced the basic observed seasonal nutrient cycles: high in winter, low in summer, and transitional in spring and autumn. On the Scotian Shelf (SR9), modelled nitrogen displayed limited interannual variations in winter (coefficient of variation $CV = 0.11$ vs. 0.16 on average in the tidally dominated regions). Only in winter 2001, 2008, and 2009 was nitrogen concentration slightly higher (>10 μM) than during the other years and relatively lower (<7.5 μM) in winter 1996, 1998, and 2004. Also in autumn 1999 and 2004, nitrogen replenishment started later than in other years, resulting in relatively shorter nitrogen-replete period in the following year. For the other tidally dominated regions including the Bay of Fundy (BF; SR2), GOM coast (SR3), GB (SR4), and NS (SR5), nitrogen concentration in winter 1998 was lower compared with other years. Particularly in the coastal region and on NS, the nitrogen level in winter 1998 was only half of that in 1999. There was also a drop in nitrogen level in winter 2005 when compared with 2004. NS showed the highest interannual variability in nitrogen level in winter with a *CV* of

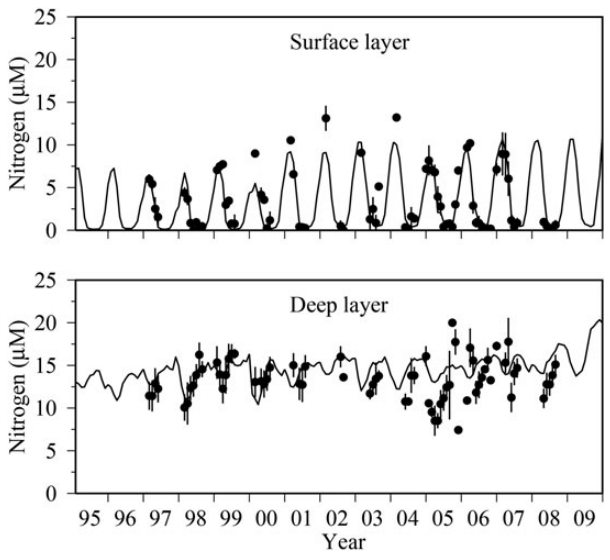

Figure 7. Model-predicted nitrogen (lines) vs. historical data (dots) in the deep GOM (SR6–SR8). Vertical bars indicate the standard deviation.

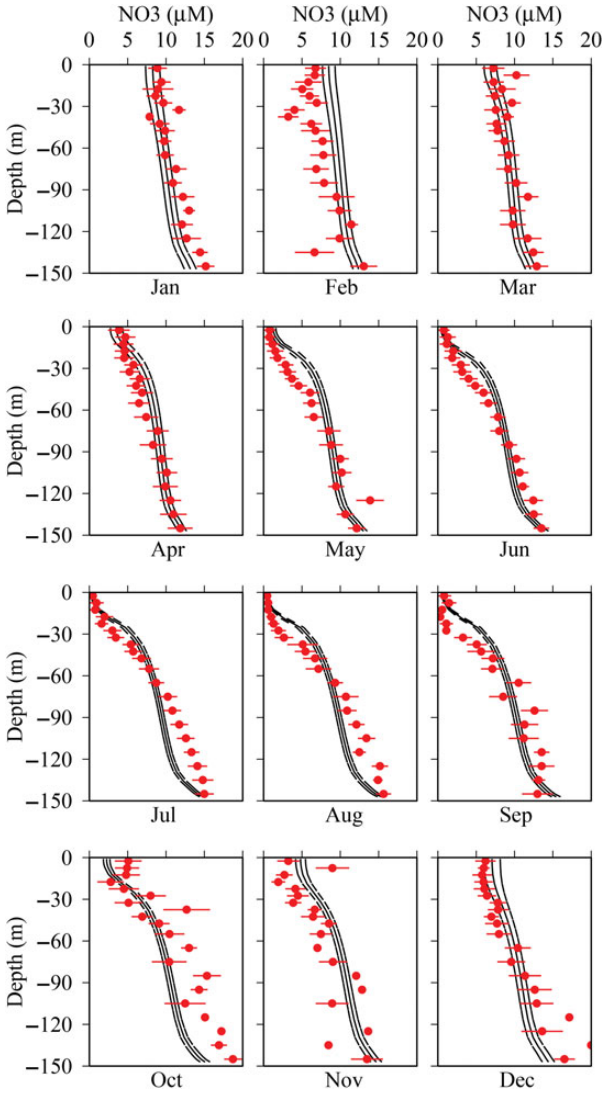

Figure 8. Nitrogen profile in the GOM (SR6–SR8). Red dots are monthly averages of historical data and the horizontal bars are the standard deviations. Solid lines are the average of model prediction from 1995 to 2009 and the dashed lines indicate the standard deviation of model prediction.

0.25 over the 15 winters, whereas the average *CV* of the other tidally dominated subregions was 0.15.

For the deep Gulf region (SR6–SR8), nitrogen displayed seasonal and interannual variations in the surface layer similar to that observed in the shallow regions (Figure 7). Seasonal variation was basically dominated by nitrogen replenishment in winter and depletion in summer. On the interannual scales, winter 1998 was also characterized by relatively low nitrogen in the surface layer as that observed in the shallow regions. There was also a decline of nitrogen concentration in winter 2005 compared with that of 2004, but it was in 2000, when the lowest level of nitrogen was observed. In general, the model results compared relatively well with the historical data, but some particularly high values were not reproduced, such as in winter 2002 and 2004. The model results were averaged over the large subregions, whereas the data were collected at specific locations. Spatial variations can also create deviation in the model–data comparison. The deep layer showed much less variations than the surface layer ($CV = 0.11$ in the deeper layer vs. 0.96 in the surface layer over all seasons and years). Although seasonal variations in the deep layer were limited, nitrogen concentration decreased during the replenishment in surface water in winter, indicating that nitrogen was brought from deeper to the surface layer due to increased vertical mixing. Nitrogen increase in summer in the deep layer most likely resulted from remineralization of sinking biogenic detritus that conveyed material flux from the surface euphotic zone to deep water. In general, the model results compared relatively well with the data in the deep layer, but tended to underestimate the interannual variations. Particularly from 2005 to 2008, data tended to show more seasonal variations than the model prediction.

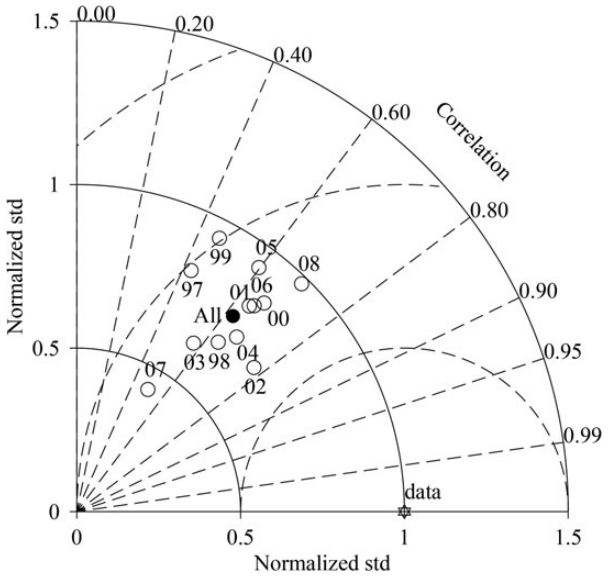

Figure 9. Nitrogen Taylor diagram based on historical data and model prediction 1997–2008 (no data available for other years). Star, data; dot, all years combined; number, year. Modelled results were interpolated to the data points in space and time in the simulation domain. The number of data samples varied from 121 in 1997 to 2699 in 2001 with a total of 15 060 in the all years combined case. The correlation coefficient R for significance at 95% confidence for Student's t-test is >0.15 for a sample size of 121 and >0.01 for a sample size of 15 060 ($t = R\sqrt{n-2}/\sqrt{1-R^2}$ where n is the sample size).

Monthly nitrogen profiles were established in the GOM based on the subregional average (SR6–SR8) of both available data and model results to illustrate the vertical structure and similarity between simulation and observation (Figure 8). Nitrogen was

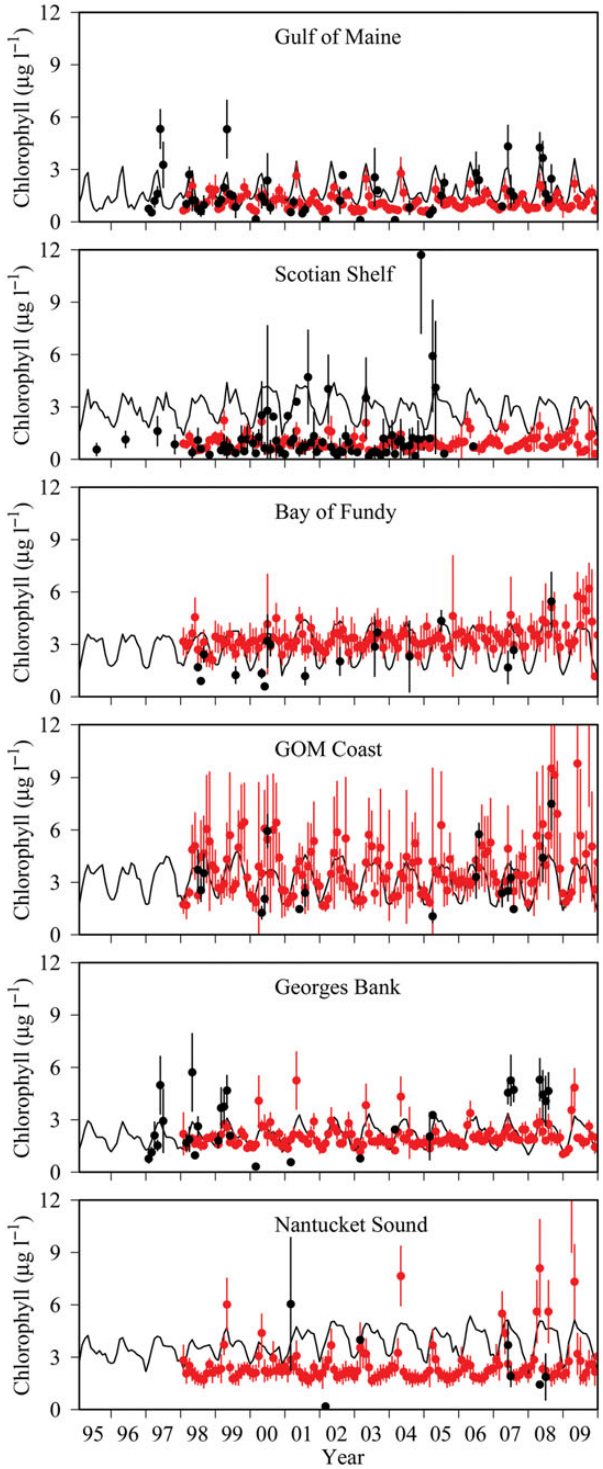

Figure 10. Model-predicted chlorophyll (black lines) vs. historical data (black dots) and SeaWiFS estimates (red dots) for the six subregions SR6–SR8, SR9, and SR2–SR5. Vertical bars indicate the standard deviation.

relatively high in surface layers in winter (January–March) and increased gradually from surface to bottom layers. Nitrogen removal essentially started in April and a subsurface nutricline formed as a result of nitrogen removal and wind-induced mixing. Nitrogen removal from the surface layer continued from April through June when the surface nitrogen level dropped practically to zero with the nutricline gradually deepening. The nutricline stayed at a similar level from July through September and nitrogen started to be replenished in October till December when the nitrogen vertical profile resembled that in January. The model results were mostly comparable with the data in terms of vertical structure and seasonal variations.

A Taylor diagram was constructed based on all nitrate data in the simulation domain. Moulded results were interpolated to the data points in space and time before statistical analysis. The number of data samples varied from 121 in 1997 to 2689 in 2001 with a global total of 15 060 for all the years combined. The correlation coefficient between observed and simulated nitrogen concentration ranged between 0.4 and 0.8, all highly significant based on Student's *t*-test (Figure 9). The highest correlation coefficient (0.8) was found for the year 2002 and the lowest value (0.4) for 1997. The global correlation coefficient for all the years combined was 0.63. The standard deviation (STD) of the model prediction was relatively smaller than that of the data for all the years and the combined dataset. The highest normalized standard deviation (the ratio between the model STD and data STD) was found for the year 2008 when the STD was similar between the model prediction and observation. The lowest normalized STD was found for the year 2007 when the model-predicted variability in nitrogen concentration was approximately half of the observed value. For the other years, the normalized STD of model prediction ranged from 0.63 to 0.94 and 0.77 for all years combined. The difference between model prediction and observation (i.e. the distance between the data point and individual years in the Taylor diagram) ranged from 0.6 to 1 times the STD of the data. For all years combined, the centred RMSE was 0.79 times the data STD. Given the variation in the data, these residuals between simulation and data are within a plausible range.

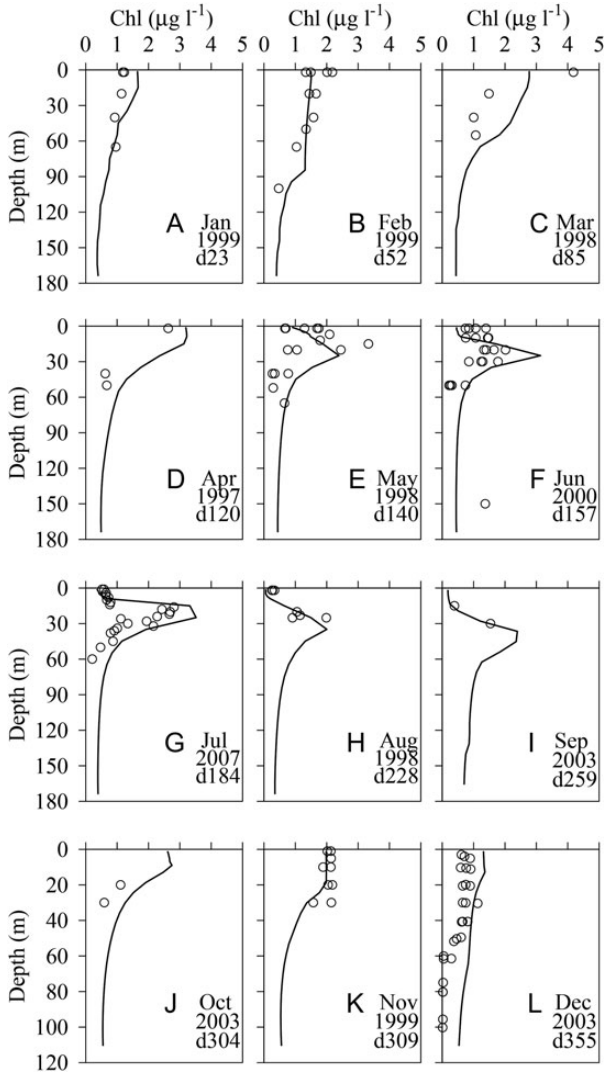

Figure 11. Examples of profile comparisons between simulation (lines) and data (circles) in Wilkinson Basin (SR8) for each month. Year and date (d#) of sampling are noted on each panel. No data are available from September through December in Wilkinson Basin and panels I–L show data on the Scotian Shelf (SR9).

Chlorophyll

As few synoptic data of phytoplankton biomass were available, modelled results of phytoplankton biomass were converted to chlorophyll by using the C:Chl. ratio of 50 and the Redfield C:N ratio of 6.625 (Anderson, 2009) and then compared with field observation and SeaWiFS data. For visual comparison, monthly average and standard deviation of historical data and SeaWiFS data were plotted against model prediction for the six subregions SR6–SR8, SR9, and SR2–SR5 (Figure 10). For the deep Gulf region, model prediction and data compared relatively well. The seasonal pattern was characterized by a dominant spring bloom and a relatively small autumn bloom. In certain cases, field measured values were higher than SeaWiFS estimates such as in 1997, 1999, 2007, and 2008. The model prediction was mostly between the two previous estimates.

In the shallow regions with either high tidal energy dissipation (SR2–SR5) or inflow from the upstream (SR9), a common feature is that there was no prominent spring bloom when compared with that in the deep Gulf (SR6–SR8). Instead, elevated chlorophyll concentration occurred from spring until autumn. On the Scotian Shelf, there was a gradual decrease in chlorophyll concentration from spring to autumn. Data from field measurement were higher than SeaWiFS estimates in certain cases and the model prediction was mostly comparable at the upper boundary of field observation. This area is close to the open boundary and under the influence of the inflow from the eastern Scotian Shelf and boundary conditions. In the BF, model prediction and data compared fairly well. Only in 2009 were the SeaWiFS data notably higher than the model prediction and also higher than the other years. In the BF and other coastal areas, nutrient loadings from river discharge add another dimension of complexity that can cause mismatches between model and observation.

In the GOM coastal region, SeaWiFS revealed particularly high variability in chlorophyll concentration, and usually, the SeaWiFS estimates were higher than field observations. Model prediction was mostly comparable with field data and also within the low range of SeaWiFS estimates. On GB, model-SeaWiFS data compared relatively well. In 2007 and 2008, however, historical data showed values higher than both SeaWiFS data and model prediction. Historical data were also scattered from 1997 to 1999, with

SeaWiFS estimates and model prediction within the range of field data variations. There were few historical chlorophyll data in Nantucket Shoals (NS). SeaWiFS data also showed large variation in certain years. The model prediction was higher than SeaWiFS data at the low range, but lower than the SeaWiFS data at the high range. NS is a particularly active tidal-energy-dissipation zone where tidal waves from the GOM and south NES converge (Shearman and Lentz, 2004; Chen *et al.*, 2011). The complex hydrodynamics can potentially influence the ecosystem function and result in high variability.

To further examine vertical structure in the water column, examples of chlorophyll profiles were presented together with model predictions (Figure 11). These profiles were selected each month to show seasonal variations in the Wilkinson Basin (SR8). Chlorophyll concentration was relatively low in the entire water column in January and February. An increase in chlorophyll concentration was observed and also simulated in the surface layer in March and April, followed by a subsurface maximum in May that was observed and predicted, which lasted until September. The depth of the subsurface maximum gradually deepened from around 20 m in May to ~40 m in September. Chlorophyll concentration increased again in October, followed by a decrease in November, returning to winter chlorophyll level in December. The model prediction compared well with the data and in particular, the amplitude and depth of the subsurface chlorophyll maximum matched well between the model and the data.

A Taylor diagram was constructed on the monthly data averaged over the entire simulation domain (Figure 12). The correlation coefficient ranged from 0.41 in 1998 to 0.77 in 2007 and 0.53 for all years combined. The one-tail Student's *t*-test gives a minimum correlation coefficient for 95% significance of 0.50 for a sample size 12 for individual years and 0.14 for a sample size of 144 for the all-years combined case. Except for the years 1998 and 2000, all other years have a significant correlation coefficient between observation and simulation. In terms of variations, the standard deviation (STD) of simulation was higher than that of SeaWiFS data in most of the years. Only in 2009, the simulated STD was smaller than that of the SeaWiFS data. For the other years, the normalized STD ranged from 1.07 in 1999 to 1.86 in 2005. For all years combined, the variability of model prediction and SeaWiFS data was comparable, with an STD ratio of 1.1. Considering the difference between model prediction and SeaWiFS data, the centred RMSE ranged from 0.78 (2009) to 1.38 (2002) times the STD of the SeaWiFS data. For all years combined, the difference stood at the same level of the SeaWiFS data STD.

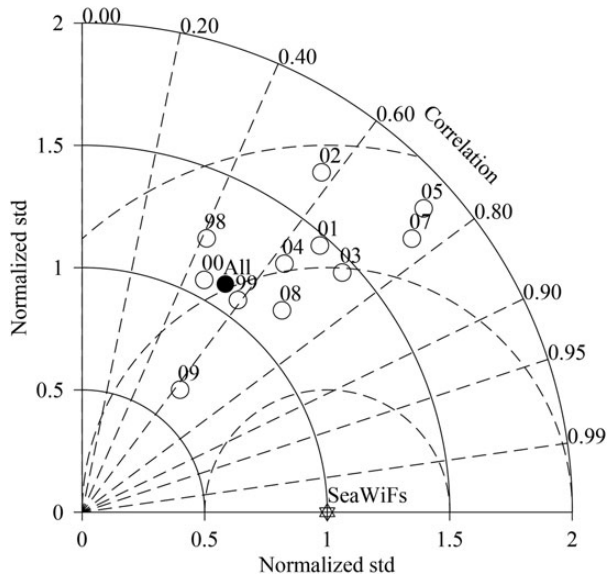

Figure 12. Taylor diagram based on monthly SeaWiFS and modelled chlorophyll concentration from 1998 to 2009 averaged over the whole domain. Star, SeaWiFS; dot, all years combined; number, year. The correlation coefficient *R* for significance at 95% confidence for Student's *t*-test is >0.50 for a sample size of 12 and >0.14 for a sample size of 144 in the all-years combined case.

EOF analysis

An EOF analysis of primary production was performed to synthesize the spatial structure and time evolution of phytoplankton production process. It is worth noting that in the physical simulation, the model bathymetry was cut off at 300 m off-the-shelf break connecting to the interior of the Atlantic Ocean. These regions were subject to the specified open boundary condition where no Gulf Stream and water transport from the upstream Labrador Sea were included. The model cannot adequately resolve these regions in terms of both physical and biological fields. Consequently, we removed these regions in the EOF analysis (Figure 13).

The EOF analysis results show that the phytoplankton field variability is well characterized by the first and second modes, which account for 67 and 14% of the total variance, respectively. The third and fourth modes contributed only 3 and 2% to the total variance, which were not significant. Mode 1 (Figure 13a) essentially represents the shallow tidally dominant system including the southwestern Scotian Shelf, BF, GOM coastal region, GB, and NS (SR1–SR5 in Figure 1). These five regions are highly tidally dissipated and vertically well mixed (Chen *et al.*, 2011). The Mode 1 amplitude time-series (Figure 13c) exhibited high values in spring through early autumn and low values in later autumn and winter. This pattern has certain similarity with the chlorophyll concentration, which had relatively high values from spring through early autumn. Based on the Mode 1 time-series, the persistent high level in chlorophyll concentration was essentially sustained by elevated primary production rate during a long period.

EOF Mode 2 essentially represents the deep Gulf region (SR6–SR8), Scotian Shelf (SR9), and shelf break zone (Figure 13b). The deep Gulf region, the region between the 60- and 200-m isobaths on the Scotian Shelf, and the shelf break zone over the southern NES show higher loading, while the southern flank and the Northeast Peak of GB between the 60- and 200-m isobaths had modest loading on both the first and second modes, which we believe function as a transitional region. The Mode 2 amplitude time-series (Figure 13d) displayed a peak value in the spring of each year, which represents the spring phytoplankton bloom. A second peak was also seen during autumn season each year, which coincided with the autumn bloom. It is clear that the dynamics controlling the second mode were more relevant to the local air–sea interaction (in the deep GOM region) and the inflow transport from the remote upstream region (Scotian Shelf).

Discussion

The EOF analysis clearly distinguishes two different systems in terms of phytoplankton primary production. The first system is characterized by sustained high primary production from spring through early autumn. For this to happen. there must be sustained nutrient

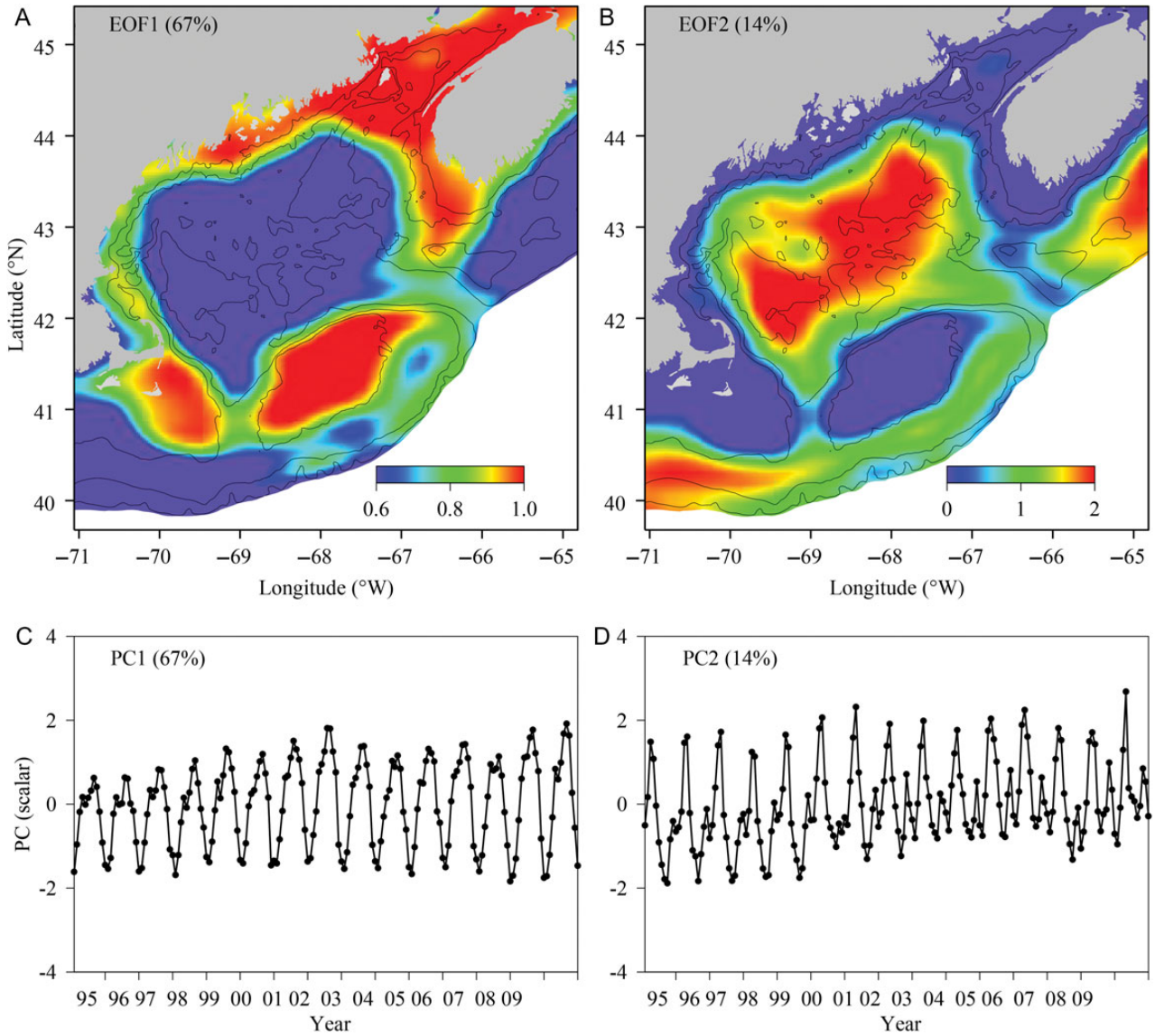

Figure 13. EOF analysis of primary production. The upper panels depict the spatial structure of the first two EOF modes and the low panels present the time-series of the first two modes (dimensionless scalar).

resources that fuel the high production. These regions are tidally dominated with high tidal energy dissipation, which can explain in part the nutrient transport system leading to the sustained high primary production. Nutrient tidal pumping resulting from multiple hydrodynamic processes is the key in nutrient supply and sustained primary production on GB (see the Introduction section). Although tidal pumping most likely affects other shallow regions, each has its own specific hydrodynamic regime. NS (SR5), in addition to tidal pumping from the GSC, is also a flow-through system without a well-defined frontal zone (Shearman and Lentz, 2003, 2004; Xue *et al.*, 2011). Due to cross-isobath currents, nutrient supply at the shelf break region can rapidly spread into the whole region. The GOM coastal subregion (SR3) is characterized by large tides and energetic tidal mixing. Interaction between tidal currents and sloping-bottom topography can generate nutrient flux from the deep Gulf region (SR6–SR8) onto the coastal region. River discharges bring additional nutrients into the system, which contribute to the elevated primary production. Besides tidal rectification and river discharge, the coastal current system (EMCC–WMCC) represents a specific feature for this subregion. The coastal current ranges from 10 to 20 cm s^{-1} and occasionally reaches up to 50 cm s^{-1} (Geyer *et al.*, 2004). Current variation and instability can generate cross-isobath nutrient transport fuelling local phytoplankton growth (Smith and Sandstrom, 1988). The exceptional high tide in the BF (SR2) and the subsequent vertical mixing is the primary factor behind the sustained phytoplankton production there. It has been reported that internal tides and soliton-like waves help to convey nutrients from deep to the surface layers (Gordon and Bretta, 1982). Grand Manan Island, located at the entrance of the BF, provides a unique topographic feature for tidal interaction and thus enhances nutrient supply and primary production (Townsend *et al.*, 2006). Two major rivers, the St John River and St Croix River, empty into the BF, contributing additional nutrient sources. The southwestern Scotian

Shelf (SR1) is a broad, curved shelf that features both large tidal currents and high energy dissipation (Chen *et al.*, 2011) and a strong coastal flow of Scotian Shelf water clockwise around Cape Sable towards the mouth of the BF (Smith, 1983; Beardsley *et al.*, 1997). The high phytoplankton production found in this subregion is fuelled by nutrients from deeper water through topographic upwelling (Tee *et al.*, 1993). They found that the large tidal currents combined with the curving isobaths and mean current (especially near Cape Sable) generated a mean cross-isobath bottom flow. This flow brought nutrients onshore into the tidal mixing zone where the water column was well mixed.

In contrast to these highly energetic regions, the central part of the GOM (SR6–SR8) is stratified during the summer season. Once the nutrient stock is taken up during the spring phytoplankton bloom, stratification impedes further significant nutrient supply from the deep layer so that phytoplankton production stays at a relatively lower level during the summer season. In late autumn, increased cooling and windstress erode the thermocline and increases vertical mixing, which bring nutrients from deeper layers to the euphotic zone and fuel phytoplankton development, leading to the autumn bloom. Although the species composition of the spring and autumn blooms may be different and these differences are not resolved by the aggregated NPZD model, we believe that the key control on the timing and amplitude of phytoplankton blooms is the physics-controlled nutrient flux and this flux was reasonably simulated by this simple NPZD model. The Scotian Shelf (SR9) is outside the GOM/GB resonant system, where the tidal amplitude is much smaller than in the GOM/GB system. This shelf is directly downstream of the Gulf of St Lawrence, the Grand Banks, and the Newfoundland/Labrador shelves. The dynamics controlling the primary production is highly associated with wind- and buoyancy-induced regional circulation and shelf-basin water exchanges.

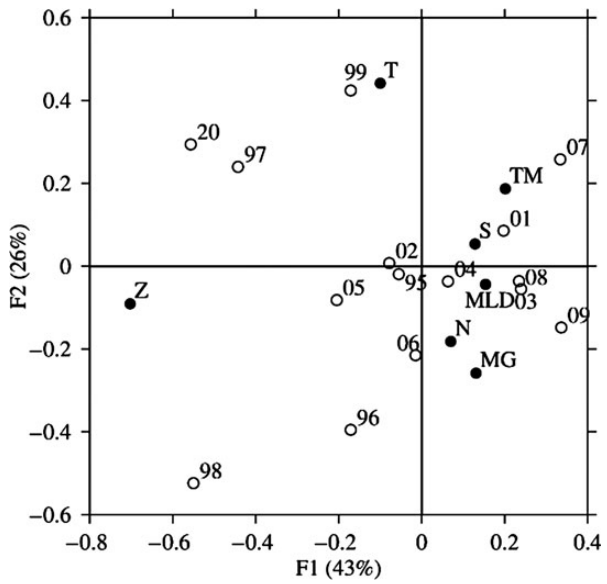

Figure 14. Correspondence analysis of the timing (TM) and magnitude (MG) of the spring bloom, winter mixed layer depth (MLD), nitrogen concentration (*N*), zooplankton abundance (*Z*), temperature (*T*), and salinity (*S*). The first and second principal axes are labelled F1 and F2, respectively. Numbers are the years without the centennial numbers except 2000 which is indicated by the centennial number (20).

The stratified deep Gulf region also shows more interannual variability in terms of annual primary production than the more energetic coastal and bank subregions. Based on the annual primary production predicted by the model, GB is the most productive subregion with average primary production of 321 g C m^{-2} $year^{-1}$ over the 15 years, followed by NS (295 g C m^{-2} $year^{-1}$), GOM coast (275 g C m^{-2} $year^{-1}$), BF (246), deep GOM (193 g C m^{-2} $year^{-1}$), and the Scotian Shelf has the lowest production (155 g C m^{-2} $year^{-1}$). On an interannual level, the annual primary production ranged from 154 to 223 g C m^{-2} $year^{-1}$ in the deep Gulf region and from 248 to 315 g C m^{-2} $year^{-1}$ in the GOM coastal region. GB, on the other hand, showed the smallest interannual variation, with annual primary production between 280 and 355 g C m^{-2} $year^{-1}$. This is not surprising since the on-bank transport of nutrients from the deeper GOM is due primarily to tidal pumping and other tidally driven and non-linear processes. As tidal energy does not change over years, although the area of the vertically well-mixed region bounded by the tidal mixing front changes seasonally, these regions show a resilience in terms of interannual variability.

The Wilkinson Basin (SR8) is a typical deep stratified region in which regular spring phytoplankton blooms occur each year. A correspondence analysis was conducted to investigate the dynamics of the spring phytoplankton bloom, interannual variability, and controlling factors. The analysis included the timing and amplitude of the spring bloom, winter surface mixed layer depth, temperature, salinity, zooplankton abundance, and nitrogen level in terms of a basin average (Figure 14). The timing of the spring bloom ranged from day 86 in 2005 to day 124 in 2007 and the magnitude ranged from 4.0 μg chl l^{-1} in 1997 to 5.8 μg chl l^{-1} in 2008. The first and second principal components of the correspondence analysis explain 43 and 26% of the total variance, respectively, which are quite significant in terms of variance representation. Bloom timing and amplitude, mixed layer depth, and nitrogen are all clustered on the positive side of the first principal axis. This suggests that the deeper mixed layer delays the spring phytoplankton bloom, but the abundance of nutrients resulted from strong vertical mixing leads to a stronger bloom. On the other hand, zooplankton is loaded on the negative side of the first principal axis, which typically indicates a top-down control in phytoplankton development. Since vertical migration, winter diapauses and predation from high trophic levels were not simulated in the model (Johnson *et al.*, 2006), zooplankton results should be interpreted with caution, although it was consistent with the Continuous Plankton Recorder data reported in Kane (2011). Salinity is grouped together with the mixed layer depth, nitrogen concentration, and the timing and amplitude of the spring phytoplankton bloom, but temperature is isolated on the second principal axis. Consequently, salinity is the primary factor in determining the dynamics of the spring phytoplankton bloom in the GOM. Freshwater inflow is one of the key elements in determining stratification and the onset of the bloom in some parts of the Gulf (Ji *et al.*, 2007, 2008). There are two major freshwater sources for GOM: local sources from rivers and external sources from the Scotian Shelf. The physical model included 33 rivers emptying into the entire Gulf. External sources include the low-salinity Labrador Current and the Gulf of Saint Lawrence.

If one rotates the principal component axes 45° anticlockwise, then axis 1 will be closely aligned along the line from point 1998 to point 2007, with salinity in the positive side in 2007 but negative side in 1998. Indeed, 1998 is characterized with low salinity (31.45), a relatively shallow winter mixed layer (90 m), and a relatively earlier

phytoplankton bloom (on day 90). Greene and Pershing (2003) showed that the freshening in 1998 was essentially a remote-controlled event through the inflow on the Scotian Shelf, although the exact sources and mechanisms are still not well understood. Li *et al.* (2014) recently suggested that wind-induced interannual variability of shelf-water transport affects the surface salinity on the NW Atlantic shelf region as well.

Based on our model prediction, this event altered the timing and magnitude of the spring phytoplankton bloom in the GOM. The years 2001 and 2007 are now located on the positive side of the rotated first principal axis, together with salinity. These two years are characterized with high salinity (33.2 and 33.34, respectively), deeper winter mixed layers (193 and 159 m), high nutrient levels (10 and 11 $\mu M\, l^{-1}$), and later spring blooms (on day 111 and 124, respectively). All 3 years from 1998 to 2000 are located on the negative side of the first principal axis. This indicates that the 1998 freshening event lasted through 2000. The year 2001 appears a recovery year from this major freshening event. The years 2005 and 2006 are also on the opposite side of salinity on both the (non-rotated) first and second principal axes, though with a shorter distance when compared with 1998. These two years are also characterized with relatively low salinity (32.4 and 32.8, respectively) and earlier spring blooms (on days 86 and 90). This freshening event is much weaker than that in 1998 and the system recovered in 2007. Salisbury *et al.* (2009) reported that spring 2005 was among the wettest on record for the drainage basins discharging into the Gulf including the Gulf of Saint Lawrence. As such, local river discharges appear the major source for the freshening event in 2005. Regardless of the origin of freshwater, both freshening events affected the timing and amplitude of the spring bloom.

Given that the same outer boundary conditions were used for all years, the model appeared to resolve some of the interannual variability caused by the boundary inflow. The nutrient concentration can vary in the inflow from the Scotian Shelf, and in particular, in the slope water that enters into the GOM through the NEC. Petrie and Yeats (2000) reported that the cold-fresh Labrador Current is characterized with low nutrient when compared with warm offshore slope waters. Nitrate concentration is >23 μM in the Warm Slope Water, but only 15–16 μM in cold Labrador Slope Water (Townsend *et al.*, 2006). As there were not enough data to establish boundary conditions for each year, the potential influence of nutrient concentration variations at the open boundary on the productivity and ecosystem function were not resolved in this model application.

It should be pointed out here that the simplified and aggregated NPZD model was not able to capture biological regime shift due to physical and climate forcing. It may require a more complicated model to simulate the potential impact of physical forcing on succession in phytoplankton and zooplankton species and foodweb structure. In addition, the model-produced interannual variability needs to be interpreted with caution since the physical model results used in this study do not well resolve the boundary flux associated with the inflow from the remote upstream region or the interaction with the Gulf Stream. Larger simulation domains or global–regional nested model systems are required to more adequately resolve these remote forcings, which the UMASSD/WHOI team is targeting in an ongoing project.

Summary

Our model experiment clearly distinguishes two dominant ecosystem functionalities in the GOM–GB regions. One is characterized with sustained primary production and chlorophyll concentration from spring through autumn, and the other is characterized by a prominent spring phytoplankton bloom followed by a small autumn bloom. The first functionality was found over the southwestern Scotian Shelf, GB, NS, the BF, and the GOM coastal region. These subregions are characterized by high tidal energy dissipation, which can explain in part the nutrient transport system leading to the sustained high primary production, although the detailed mechanisms can differ from region to region. The high phytoplankton production found in the southwestern Scotian Shelf is fuelled by nutrients from deeper water primarily through topographic upwelling. Tidal pumping and cross-frontal transport are the dominant dynamics leading to high sustained nutrient supply and primary production on GB. NS is essentially a flow-through system where the WMCC carries nutrients from the western GOM region into the system. In this subregion, the tidal pumping-supplied nutrients from the northern GSC could be quickly spread over the NS and lead to local high phytoplankton production. Strong vertical mixing driven by the energetic tides in the BF is the key mechanism underneath high primary production, whereas the Eastern and WMCCs, frontal instability, and river discharge contribute to high productivity in the GOM coastal regions. The second functionality was essentially identified in the deep Gulf, Scotian Shelf, and slope regions. Strong stratification in summer impedes nutrient supply and primary production, giving prominence to distinct phytoplankton blooms in spring and autumn.

Between regions of typical functionality are transitional zones where signals of both functionalities are observable but not as prominent as in the aforementioned subregions. The Northeast Peak and the southern flank of GB are found as transitional zones.

As the tides are the primary driving force in the first type of ecosystem function in which sustained phytoplankton production was simulated, these regions show limited interannual variability. On the other hand, the second type of ecosystem function where spring and autumn phytoplankton blooms were observed exhibits more interannual variations in terms of the timing and magnitude of the spring phytoplankton bloom and annual primary production. Salinity regime changes resulting from freshening events are shown to be one of the key driving factors in determining the time and magnitude of the spring bloom. During both the remotely controlled freshening event in 1998 and more locally driven freshening event in 2005, small and earlier spring blooms were simulated.

Acknowledgements

This study was supported by the US GLOBEC/Georges Bank Program through NOAA Grant NA 160P2323 and NSF grants OCE0234545, 0227679, 0606928, and 0814505 and Pan-Regional GLOBEC Program grants OCE 0814505. The authors thank Drs D. Townsend (University of Maine) and P. Clement (Bedford Institute of Oceanography) for providing us with the historical data. Two reviewers provided comments and questions that helped us improve this paper.

References

Anderson, L. A. 2009. The seasonal nitrogen cycle in Wilkinson Basin, Gulf of Maine, as estimated by 1-D biological model optimization. Journal of Marine Systems, 78: 77–93.

Beardsley, R. C., Butman, B., Geyer, W. R., and Smith, P. 1997. Physical oceanography of the Gulf of Maine: an update. *In* Proceedings of the Gulf of Maine Ecosystem Dynamics Scientific Symposium and

Workshop Report 97-1, pp. 39–52. Reg. Assoc. for Res. in the Gulf of Maine, Hanover, NH–.

Burchard, H., and Bolding, K. 2001. Comparative analysis of four second-moment turbulence closure models for the oceanic mixed lay. Journal of Physical Oceanography, 31: 1943–1968.

Butman, B., Beardsley, R. C., Magnell, B., Frye, D., Vrmersch, J. A., Schlitz, R., Limeburner, R., *et al.* 1982. Recent observations of the mean circulation on Georges Bank. Journal of Physical Oceanography, 12: 569–591.

Chapman, D. C., and Beardsley, R. C. 1998. On the origin of shelf water in the Middle Atlantic Bight. Journal of Physical Oceanography, 19: 384–391.

Chen, C., and Beardsley, R. 2002. Cross-frontal water exchange on Georges Bank: modeling exploration of the US GLOBEC/Georges Bank phase III study. Journal of Oceanography, 58: 403–420.

Chen, C., Beardsley, R. C., and Cowles, G. 2006. An unstructured grid, finite-volume coastal ocean model (FVCOM) system. Special Issue entitled "Advance in Computational Oceanography", Oceanography, 19: 78–89.

Chen, C., Huang, H., Beardsley, R. C., Liu, H., Xu, Q., and Cowles, G. 2007. A finite-volume numerical approach for coastal ocean circulation studies: comparisons with finite difference models. Journal of Geophysical Research, 112: C03018. doi:10.1029/2006JC003485.

Chen, C., Huang, H., Beardsley, R. C., Xu, Q., Limeburner, R., Gowles, G., Sun, Y., *et al.* 2011. Tidal dynamics in the Gulf of Maine and New England Shelf: an application of FVCOM. Journal of Geophysical Research, 116: C12010. doi:10.1029/2011JC007054.

Chen, C., Malanotte-Rizzoli, P., Wei, J., Beardsley, R. C., Lai, Z., Xue, P., Lyu, S., *et al.* 2009. Application and comparison of Kalman filters for coastal ocean problems: an experiment with FVCOM. Journal of Geophysics Research, 114: C05011. doi:10.1029/2007JC004548.

Chen, C., Qi, J., Li, C., Beardsley, R. C., Lin, H., Walker, R., and Gates, K. 2008. Complexity of the flooding/drying process in an estuarine tidal-creek salt-marsh system: an application of FVCOM. Journal of Geophysical Research, 113: C07052. doi:10.1029/2007jc004328.

Chen, C. S., Beardsley, R. C., and Limeburner, R. 1995. Numerical study of stratified tidal rectification over finite-amplitude of banks. Part II: Georges Bank. Journal of Physical Oceanography, 25: 2111–2128.

Chen, C. S., Liu, L., and Beardsley, R. C. 2003. An unstructured grid, finite-volume, three-dimensional, primitive equation ocean model: application to coastal ocean and estuaries. Journal of Atmospheric and Oceanic Technology, 20: 159–186.

Cowles, G. W., Lentz, S. J., Chen, C. S., Xu, Q., and Beardsley, R. C. 2008. Comparison of observed and model-computed low frequency circulation and hydrography on the New England Shelf. Journal of Geophysical Research, 113: C09015. doi:10.1029/2007JC004394.

Fennel, K., Wilkin, J., Levin, J., Moisan, W. J., O'Reilly, J., and Haidvogel, D. 2006. Nitrogen cycling in the Middle Atlantic Bight: results from a three-dimensional model and implications for the North Atlantic nitrogen budget. Global Biogeochemical Cycle, 20: GB3007. doi:10.1029/2005GB002456.

Franks, P. J. S., and Chen, C. 1996. Plankton production in tidal fronts: a model of Georges Bank in summer. Journal of Marine Research, 54: 631–651.

Franks, P. J. S., and Chen, C. 2001. A 3-D prognostic numerical model study of the Georges Bank ecosystem: Part II: biological-physical model. Deep Sea Research II, 48: 457–482.

Friedland, K. D., Hare, J. A., Wood, G. B., Col, L. A., Buckley, L. J., Mountain, D. G., Kane, J., *et al.* 2008. Does the fall phytoplankton bloom control recruitment of Georges Bank haddock, *Melanogrammus aeglefinus* through parental condition? Canadian Journal of Fisheries and Aquatic Sciences, 65: 1076–1086.

Gao, G., Chen, C., Qi, J., and Beardsley, R. C. 2011. An unstructured-grid, finite-volume sea ice model: development, validation and application. Journal of Geophysical Research, 116: C00D04. doi:10.1029/2010JC006688.

Garfield, N., III, and Evans, D. L. 1987. Shelf water entrainment by Gulf Stream warm-core rings. Journal of Geophysical Research, 92: 13003–13012.

Garrett, C. 1972. Tidal resonance in the Bay of Fundy and Gulf of Maine. Nature, 238: 441–443.

Garrett, C. J. R., and Loder, J. W. 1981. Circulation and fronts in continental shelf seas. Philosophical Transactions of the Royal Society of London, 302: 563–581.

Geyer, W. R., Signell, R. P., Fong, D. A., Wang, J., Anderson, D. M., and Keafer, B. A. 2004. The freshwater transport and dynamics of the western Maine coastal current. Continental Shelf Research, 24: 1339–1357.

Gordon, D. C., and Bretta, J. W. 1982. A preliminary comparison of two turbid coastal systems: the Dollard (Netherlands-FRG) and the Cumberland Basin (Canada). Hydrobiological Bulletin, 16: 255–267.

Gottelli, N. J., and Ellison, A. M. 2004. A Premier of Ecological Statistics. Saumer, Sunderland, MA. 510 pp.

Greene, C. H., and Pershing, A. J. 2003. The flip-side of the North Atlantic Oscillation and modal shifts in slope-water circulation patterns. Limnology and Oceanography, 48:319–322.

Header, E. J. H., Brickman, D., and Harris, L. R. 2005. An exceptional haddock year class and unusual environmental conditions on the Scotian Shelf in 1999. Journal of Plankton Research, 27: 597–602.

Hendry, R., and He, I. 1996. Technical report on objective analysis (OA) project. Bedford Institute of Oceanography, Dartmouth, Nova Scotia. 105 pp.

Horne, E. P. W., Loder, J. W., Harrison, W. G., Mohn, R., Lewis, M. R., Irwin, B., and Platt, T. 1989. Nitrate supply and demand at the Georges Bank tidal front. Scientia Marina, 53: 145–158.

Hu, S., Townsend, D. W., Chen, C., Cowles, G., Beardsley, R. C., Ji, R., and Hounghton, R. W. 2008. Tidal pumping and nutrient fluxes on Georges Bank: a process-oriented modeling study. Journal of Marine System, 74: 528–544.

Ji, R., Davis, C., Chen, C., Townsend, D. W., Mountain, D. G., and Beardsley, R. C. 2007. Influence of ocean freshening on shelf phytoplankton dynamics. Geophysical Research Letters, L24607. doi:10.1029/2007GL032010.

Ji, R., Davis, C., Chen, C. S., Townsend, D. W., Mountain, D. G., and Beardsley, R. C. 2008. Modeling the influence of low-salinity water inflow on winter–spring phytoplankton dynamics in the Nova Scotian Shelf–Gulf of Maine region. Journal of Plankton Research, 30: 1399–1416.

Ji, R. B., Chen, C. S., Franks, P. F. S., Townsend, D. W., Durbin, E. G., Beardsley, R. C., and Lough, R. G. et al. 2006. The impact of Scotian Shelf Water "cross-over" on the plankton dynamics on Georges Bank: a 3-D experiment for the 1999 spring bloom. Deep Sea Research II, 53: 2684–2707.

Johnson, C., Pringle, J., and Chen, C. 2006. Transport and retention of dormant copepods in the Gulf of Maine. Deep Sea Research II, 53: 2520–2536

Kane, J. 2011. Multiyear variability of phytoplankton abundance in the Gulf of Maine. ICES Journal of Marine Science, 68: 1833–1841.

Lai, Z., Chen, C., Cowles, G., and Beardsley, R. C. 2010. A non-hydrostatic version of FVCOM, Part II: mechanistic study of tidally generated nonlinear internal waves in Massachusetts Bay. Journal of Geophysical Research-Oceans, doi:10.1029/2010JC006331.

Li, Y., Ji, R., Fratantoni, P. S., Chen, C., Hare, J. A., Davis, C. S., and Beardsley, R. C. 2014. Wind-induced interannual variability of sea level slope, along-shelf flow and surface salinity on the Northwest Atlantic shelf. Journal of Geophysical Research, doi: 10.1002/2013JC009385.

Loder, J. W., and Horne, E. P. W. 1991. Skew eddy fluxes as signatures of non-linear tidal current interactions, with application to Georges Bank. Atmosphere-Ocean, 29: 517–546.

Marsden, I. R. F. 1986. The internal tide on Georges Bank. Journal of Marine Research, 44: 35–50.

Mellor, G. L., and Yamada, T. 1982. Development of a turbulence closure model for geophysical fluid problems. Reviews of Geophysics and Space Physics, 20: 851–875.

O'Reilly, J. E., Evans-Zetlin, C. E., and Busch, D. A. 1987. Primary production. *In* Georges Bank, pp. 220–233. Ed. by R. H. Backus, and D. W. Bourne. MIT Press, Cambridge, MA.

Petrie, P., and Yeats, P. 2000. Annual and interannual variability of nutrients and their estimated fluxes in the Scotian Shelf–Gulf of Maine region. Canadian Journal of Fisheries and Aquatic Sciences, 57: 2536–2546.

Platt, T., Fuentes-Yaco, C., and Frank, K. T. 2003. Spring algal bloom and larval fish survival. Nature, 423:398–399.

Platt, T., Gallegos, C. L., and Harrison, W. G. 1980. Photoinhibition of photosynthesis in natural assemblages of marine phytoplankton. Journal of Marine Research, 38: 687–701.

Ryan, J. P., Yoder, J. A., and Townsend, D. W. 2001. Influence of a Gulf Stream warm-core ring on water mass and chlorophyll distributions along the Southern Flank of Georges Bank. Deep Sea Research II, 48: 159–178.

Salisbury, J., Vandemark, D., Hunt, C., Campbell, J., Jonsson, B., Mahadevan, A., McGillis, W., *et al.* 2009. Episodic riverine influence on surface DIC in the coastal Gulf of Maine. Estuarine Coastal and Shelf Science, 82: 108–118.

Shearman, K., and Lentz, S. J. 2003. Dynamics of mean and subtidal flow on the New England shelf. Journal of Geophysical Research, 108: C8. doi:10.1029/2002JC001417.

Shearman, K., and Lentz, S. J. 2004. Observations of tidal variability on the New England shelf. Journal of Geophysical Research, 109: C06010. doi:10.1029/2003JC001972.

Smith, P. C. 1983. The mean and seasonal circulation off southwest Nova Scotia. Journal of Physical Oceanography, 13: 1034–1054.

Smith, P. C., Flagg, C. N., Limeburner, R., Fuentes-Yaco, C., Hannah, C., Beardsley, R. C., and Irish, J. D. 2003. Scotian shelf crossover during winter/spring, 1999. Journal of Geophysical Research, 108: 8013. doi:10.1029/2001JC001288.

Smith, P. C., and Sandstrom, H. 1988. Physical Processes at the Shelf Edge in the Northwest Atlantic. Journal of Northwest Atlantic Fishery Science, 8: 5–13.

Taylor, K. E. 2001. Summarizing multiple aspects of model performance in a single diagram. Journal of Geophysical Research, 106: 7183–7192.

Tee, K. T., Smith, P. C., and LeFaivre, D. 1993. Topographic Upwelling off Southwest Nova Scotia. Journal of Physical Oceanography, 23: 1703–1726.

Tian, R. C., and Chen, C. 2006. Influence of model geometrical fitting and turbulence parameterization on phytoplankton simulation in the Gulf of Maine. Deep Sea Research II, 53: 2808–2832.

Tian, R. C., Vezina, A. F., Starr, M., and Saucier, F. 2001. Seasonal dynamics of coastal ecosystems and export production at high latitudes: a modeling study. Limnology and Oceanography, 46: 1845–1859.

Townsend, D. W., Thomas, A. C., Mayer, L. M., Thomas, M., and Quinlan, J. 2006. Oceanography of the Northwest Atlantic Continental Shelf. *In* The Sea, 14, pp. 119–168. Ed. by A. R. Robinson, and K. H. Brink. Harvard University Press.

Xue, P., Chen, C., and Beardsley, R. C. 2012. Observing system simulation experiments of dissolved oxygen monitoring in Massachusetts Bay. Journal of Geophysical Research, 117: C05014. doi:10.1029/2011JC007843.

Xue, P. F., Chen, C. S., Beardsley, R. C., and Limeburner, R. 2011. Observing system simulation experiments with ensemble Kalman filters in Nantucket Sound, Massachusetts. Journal of Geophysical Research, 116: C01011. doi:10.1029/2010JC006428.

Yoder, J. A., Schollaert, S. E., and O'Reilly, J. E. 2002. Climatological phytoplankton chlorophyll and sea surface temperature patterns in continental shelf and slope waters off the northeast U.S. coast. Limnology and Oceanography, 47: 672–682.

Handling editor: C. Brock Woodson